NIH Public Access
Author Manuscript
J Nucl Med. Author manuscript; available in PMC 2010 October 1.

Published in final edited form as:
J Nucl Med. 2009 October ; 50(10): 1666–1675. doi:10.2967/jnumed.109.064345.

Clinical Imaging Characteristics of the Positron Emission Mammography Camera: PEM Flex Solo II

Lawrence MacDonald[1], **John Edwards**[1,2], **Thomas Lewellen**[1], **David Haseley**[2], **James Rogers**[2], and **Paul Kinahan**[1]

[1]Radiology Department, University of Washington, Seattle, Washington

[2]Swedish Cancer Institute, Seattle, Washington

Abstract

We evaluated a commercial positron emission mammography (PEM) camera, the PEM Flex Solo II. This system comprises two 6 × 16.4 cm detectors that scan together covering up to a 24 × 16.4 cm field of view (FOV). There are no specific standards for testing this detector configuration. We performed several tests important to breast imaging, and we propose tests that should be included in standardized testing of PEM systems.

Methods: We measured spatial resolution, uniformity, counting-rate linearity, recovery coefficients, and quantification accuracy using the system's software. Image linearity and coefficient of variation at the edge of the FOV were also characterized. Anecdotal examples of clinical patient data are presented.

Results: The spatial resolution was 2.4 mm in full width at half maximum for image planes parallel to the detector faces. The background variability was approximately 5%, and quantification accuracy and recovery coefficients varied within the FOV. Positioning linearity began at approximately 13 mm from the edge of the detector housing. The coefficient of variation was significantly higher close to the edge of the FOV because of limited sensitivity in these image planes.

Conclusion: A reconstructed spatial resolution of 2.4 mm represented a significant improvement over conventional whole-body PET scanners and should reduce the lower threshold on lesion size and tracer uptake for detection in the breast. Limited-angle tomography and a lack of data corrections result in spatially variable quantitative results. PEM acquisition geometry limits sampling statistics at the chest-wall edge of the camera, resulting in high variance in that portion of the image. Example patient images demonstrate that lesions can be detected at the chest-wall edge despite variance artifacts, and fine structure is visualized routinely throughout the FOV in the focal plane. The PEM Flex camera should enable the functional imaging of breast cancer earlier in the disease process than whole-body PET.

Keywords

positron emission mammography (PEM); dedicated breast PET; breast cancer imaging

Positron emission mammography (PEM) is a technique using 2 annihilation-photon detectors and limited-angle tomographic reconstruction to image radiotracer distributions within the breast. Because of their smaller size and closer proximity to the source, dedicated PEM cameras

COPYRIGHT © 2009 by the Society of Nuclear Medicine, Inc.

For correspondence or reprints contact: Lawrence MacDonald, Radiology Department, University of Washington, 1959 NE Pacific Ave., Old Fisheries Center, Room 222, Box 357987, Seattle, WA 98195. macdon@u.washington.edu.

NIH-PA Author Manuscript
NIH-PA Author Manuscript
NIH-PA Author Manuscript

NIH-PA Author Manuscript

NIH-PA Author Manuscript

NIH-PA Author Manuscript

can provide better spatial resolution and count sensitivity than whole-body PET (WB PET). PEM is undergoing clinical trials and has been suggested for breast cancer detection, characterization, treatment planning, and assessment of response to therapy. PEM, like WB PET, provides functional imaging information. Radiographic mammography, ultrasound, and MRI primarily provide anatomic information. PEM can thus provide complementary information to conventional breast imaging modalities. Screening mammography is believed to be an important factor in recent declines in breast cancer mortality (1). Despite the successes of earlier detection by mammography, however, breast cancer is the second-leading cause of cancer-related deaths in North American women. This statistic shows a clear need for improved methods to fight breast cancer.

WB PET has been used for imaging breast cancer for many years (2-4). Modern WB PET systems typically have a reconstructed spatial resolution of 5–7 mm full width at half maximum (FWHM). In practice, however, reconstructed resolution is 10–15 mm in FWHM because of added smoothing. Partial-volume effects on these systems limit qualitative assessment and quantitative accuracy for lesions smaller than approximately 25–30 mm. This technical limitation of WB PET and the inherent variability of the disease have resulted in variable sensitivity and specificity of breast PET for lesions approximately 10 mm and smaller (3). Hence, breast lesions accurately imaged using WB PET are associated with relatively advanced disease. Ideally, cancer is treated in the early stages of the disease. The idea of dedicated PEM systems is to reduce the size threshold for accurate imaging and assist earlier intervention.

PEM was proposed in the 1990s by Thompson et al. (5) and has continued to receive attention from the research community (6-8). Some of these devices have undergone preliminary clinical testing (9-13). These tests have mostly been small in scope and have used prototype devices. Although preliminary indications are encouraging, conclusions are that larger, focused studies with mature PEM technology are required to establish a role for PEM. Even with an available array of imaging agents (14), and the evident need for improved specificity, the role of PEM in the diagnosis and treatment of breast cancer is yet to be established. At the Swedish Cancer Institute, the PEM Flex Solo II (Naviscan PET Systems, Inc.) has been used since July 2007 to image breast cancer patients who have already been diagnosed and are receiving a WB PET/CT examination.

Dedicated breast PET and PEM systems are still in the early stages of development and implementation. No camera-testing standards have been developed for these systems. As with small-animal PET scanners, conventional WB PET testing standards are inappropriate for characterizing dedicated breast imaging systems because of their distinct design. In this work, we tested several common imaging parameters using the standard clinical operating mode of the PEM Flex system. Spatial resolution, counting-rate linearity, uniformity, and recovery coefficients (RCs) were measured. In addition, we investigated properties relevant to the breast imaging application, namely imaging characteristics at the edge of the field of view (FOV), which is important for imaging posterior breast lesions.

Independently, the PEM Flex Solo II was recently characterized using the NU 4-2008 Small Animal PET Standard of the National Electrical Manufacturers Association (NEMA) (15).

MATERIALS AND METHODS

PEM Flex Solo II System

The PEM Flex Solo II has 2 opposing γ-ray imaging detectors mounted inside compression paddles used to immobilize the breast. The system is shown in Figure 1. The detectors are approximately 6 × 16.4 cm in imaging area and approximately 6 cm thick. The detectors scan across the FOV in the direction of their 6-cm dimension to cover up to 24 cm, making the

NIH-PA Author Manuscript

NIH-PA Author Manuscript

NIH-PA Author Manuscript

maximum FOV of the system 24 × 16.4 cm. The detectors are constructed from 2 × 2 × 13 mm lutetium yttrium orthosilicate scintillation crystals coupled to position-sensitive photomultiplier tubes.

The detectors are mounted on an articulating arm that rotates to allow imaging from different views. One of the detectors (the compression detector) is motor-controlled to set the distance between the 2 detectors (the compression thickness). Manual adjustment of the compression thickness is also possible. Acquisition options on the PEM Flex Solo II at the Swedish Cancer Institute include the scan range FOV (up to 24 cm), compression thickness, and acquisition duration. List-mode data are acquired continuously, and the detectors scan continuously across the FOV. The image reconstruction uses 5 iterations of a 3-dimensional list-mode maximum-likelihood expectation maximization (MLEM) algorithm. Lines of response are limited to Δx and Δy less than 52 mm (x- and y-axes are defined in Fig. 1C). This is done to minimize depth-of-interaction parallax error from obliquely incident photons. No corrections are made for scattered or accidental coincidence detections, and there are no user-selectable reconstruction filters or other options.

The PEM Flex Solo II is a limited-angle, focal-plane tomography system (tomosynthesis). Tomosynthesis has been used primarily in radiographic imaging, and the principles of the technique have been described by Dobbins and Godfrey (16). The PEM Flex detector geometry results in a collection of coincidence lines of response with limited angular sampling that can be used to reconstruct high-resolution images parallel to (in-plane images, Fig. 1C) but not perpendicular to (cross-planes) the detector faces. The underlying reason for this is that the detectors do not encircle the object, nor do they rotate to acquire the full 360° angular sampling required for fully 3-dimensional tomography. Tomosynthesis is associated with well-known problems of quantitative inaccuracy and strongly anisotropic spatial resolution. Because of the spatial anisotropy, 2 orthogonal imaging views, for example, craniocaudal and mediolateral oblique (MLO), are required to achieve high-resolution imaging in all 3 dimensions. The PEM Flex system generates in-plane images with a pixel size of 1.2 mm. There are 12 or 24 in-plane slices, making the cross-plane pixel sizes variable, determined by the detector separation divided by 12 or 24. In October 2008, the PEM Flex at the Swedish Cancer Institute received a software upgrade that changed the exported DICOM studies from 24 slices to 12 slices. The data for this work were acquired before this upgrade but retained on the acquisition computer and have been exported with both 24- and 12-slice versions of the DICOM software.

The PEM Flex Solo II reports image values either using absolute activity concentration kBq/mL (μCi/cc) or using a parameter referred to as the PEM uptake value (PUV). The PUV differs from the standardized uptake value, which is a standard metric used in WB PET (17), in that the activity concentrations measured in the PEM images are not corrected for attenuated or scattered photons. Because of this discrepancy, the manufacturer advocates evaluating image lesions using a ratio of lesion to region-of-interest (ROI) PUV divided by background ROI PUV, rather than using PUV alone as an image metric. Our results were taken from image analysis performed on the PEM Flex workstation (PEMView+, version 1.2.3), with images exported from the PEM Flex workstation in DICOM format to OsiriX (version 3.2.1) (18) and IDL (Interactive Data Language; ITT Visual Information Solutions) software.

Detector Characterization

Spatial Resolution—We measured spatial resolution by imaging 1.0-mm-inner-diameter capillary tubes that contained a small amount of ^{18}F solution. Capillary tubes were imaged at different locations within the FOV and with compression distances of 3, 6, and 9 cm. Spatial resolution was calculated on the image slice with maximum counts by fitting a profile of the line source to a gaussian curve. Profiles of the line source were always taken perpendicular to the length of the capillary tube. We point out that this determination of spatial resolution

NIH-PA Author Manuscript

NIH-PA Author Manuscript

NIH-PA Author Manuscript

deviates from the conventional method of determining spatial resolution in a PET scanner as prescribed by NEMA standards in at least 3 ways. It is recommended that spatial resolution be calculated from an image reconstructed using an analytic filtered backprojection method, whereas here we used MLEM; second, the resolution we measured was limited by the image pixel size; and third, FWHM is not determined from a gaussian fit in the NEMA standard (19).

Uniformity—We made uniform sources by injecting ^{18}F solution into intravenous saline bags at a concentration of approximately 5 kBq/mL. The source was placed in the PEM Flex FOV such that a portion of the activity distribution was outside the FOV. The source was positioned in this way to measure imaging effects at the edge of the FOV. Air was removed from the intravenous bags, and they were compressed between the detectors to a 55-mm thickness. An 18-cm-wide scan FOV was used to image the 11.8-cm-wide source for 1, 3, 7, and 15 min.

The background variability was calculated using a modified NEMA standard. Our method was to draw six 2.0-cm-diameter ROIs on each of the in-plane image slices for both the 12- and 24-slice image volumes. The background variability was calculated as specified by NEMA (19) using the 72 and 144 ROIs on the 12- and 24-slice images, respectively.

Counting-Rate Linearity—The total number of prompt events (including true, scattered, random, and intrinsic ^{176}Lu coincidence events) was recorded for 3-min acquisitions covering 18 cm using a uniform source containing different activity concentrations. The 1.0-L intravenous bag source was again placed such that a portion of the bag was outside the PEM Flex FOV; approximately 0.8 L of the 1.0-L intravenous solution was in the FOV. The detectors were set to 50-mm compression. The random coincidence counts from a delayed coincidence window were also reported. The numbers of prompt and random coincidence events reported by the PEM Flex scanner represent all events above the lower threshold set by the hardware discriminator on the detector readout. Further discrimination is performed later using an energy acceptance window (350–700 keV) applied in the system software.

We changed the activity concentration in the intravenous bag by beginning with a low concentration and then adding appropriate amounts of ^{18}F source. This method requires multiple measurements of ^{18}F activity in a dose calibrator (Atomlab-100; Biodex Medical Systems), which potentially adds uncertainty to the measured level of source concentration. However, this method was used to accommodate the clinical schedule at the Swedish Cancer Institute.

Edge Effects—Two image properties were studied at the edge of the PEM Flex FOV: the positioning limits and linearity and the coefficient of variation (COV). The COV is defined as the SD of pixel values within an ROI divided by the mean of the same ROI. The purpose of the linearity measurement was to determine the distance between the accurate imaging field and the physical edge of the detector. A line source was imaged near the detector edge to measure the limits and linearity. The COV was calculated from 1-dimensional profiles (95 mm long, along *x*-axis Fig. 1C) near the FOV edge. Only in-plane images are viewed in practice, and the 1-dimensional COV represents variance observed on the edge of these images. The COV was calculated on the uniformity images described above.

RCs—We studied 2 forms of RCs: relative RCs and absolute RCs. Relative RCs compare image values in hot-spot ROIs with image values from background regions. Absolute RCs compare activity concentrations measured in an image with the known true activity concentration in the object. It is difficult or impossible to draw ROIs within small source structures in a way that excludes surrounding background image pixels. Consequently, on patient images at the Swedish Cancer Institute, ROIs larger than the sources of interest are

NIH-PA Author Manuscript

NIH-PA Author Manuscript

NIH-PA Author Manuscript

drawn around the sources, and the maximum pixel value within the ROIs is recorded as the measure of lesion uptake. Large ROIs are also drawn around background areas of the image, away from the source of interest, and the mean of the ROI pixel values is taken as the measure of background uptake. Clinically, lesion-to-background ratios are calculated with these 2 measurements, and so this methodology was followed for the calculation of the RC in this work. We also drew ROIs completely within the hot sources in our experiments so that mean pixel values within the sphere could be determined, and we calculate a third RC parameter using the hot-spot ROI mean pixel value divided by the background ROI mean pixel value. RC are calculated as

$$\text{relative } RC_{max} = \text{maximum (hot-spot ROI)} / \text{mean (background ROI)}, \quad \text{Eq. 1}$$

$$\text{relative } RC_{mean} = \text{mean (hot-spot ROI)} / \text{mean (background ROI)}, \quad \text{Eq. 2}$$

$$\text{absolute } RC_{max} = \text{maximum (ROI activity concentration)} / \text{true (ROI activity concentration)}. \quad \text{Eq. 3}$$

We used plastic spheres filled with an activity concentration 4 times that of the background to measure RCs. We also imaged spheres with 10× background activity as a visualization-limit test. The 4× ratio was used for RC calculations according to the NEMA standard (19). Two 500-mL intravenous bags, as described earlier in the “Uniformity” section, served as the background activity. The spheres (Standard and Micro Hollow Sphere Sets; Data Spectrum Corp.) were imaged close to the center of the in-plane FOV. Imaging was performed with the spheres between the 2 intravenous bags and repeated with the spheres below the 2 intravenous bags in contact with 1 of the detectors. The background concentration was approximately 5 kBq/mL. Sphere inner diameters were (in mm) 4, 5, 8, 15, 20, 25, and 31.

In addition to measuring RCs as a function of sphere size, we measured quantification of a single source placed at 4 cardinal locations within the FOV of the PEM Flex system. We used the 2-cm-diameter sphere for this and placed it in the 4 positions shown in Figure 1C.

We made the RC and quantification measurements from ROIs drawn on the in-plane image slice with the highest mean ROI value.

Clinical Protocol

At the Swedish Cancer Institute, the PEM Flex Solo II is used to image patients who have already been diagnosed with breast cancer and are undergoing WB PET/CT. The WB PET/CT protocol included a fast of 6–12 h, blood glucose levels less than 150 mg/dL, a 600-MBq injection of ^{18}F-FDG, a 60-min uptake time, and an approximately 30-min WB PET/CT examination. Immediately after the WB PET/CT examination, the patients are taken to the PEM Flex system and imaged as follows: craniocaudal view of the contralateral breast, craniocaudal view of the ipsilateral breast, MLO view of the ipsilateral breast, and MLO view of the contralateral breast. Each acquisition was for 7 min and covered the full 24-cm-wide FOV. In most cases, a mild degree of breast compression was used to immobilize the breast. The action of compressing the breast tended to displace some tissue out of the FOV. In certain cases, especially when there was suspected involvement in the posterior breast, compression was greatly reduced or eliminated altogether to image as far posterior (close to the chest wall) as possible.

NIH-PA Author Manuscript

NIH-PA Author Manuscript

NIH-PA Author Manuscript

Examples of patient images are presented to illustrate representative clinical findings.

RESULTS

Spatial Resolution

The mean FWHM spatial resolution measured at several locations within the FOV and for 3 different compression thicknesses was 2.4 ± 0.3 mm in the in-plane images and 8.0 ± 1.0 mm in the cross-planes. Spatial resolution results are summarized in Table 1.

Uniformity

The image of the uniform source acquired for 7 min is shown in Figure 2. The detector edge appears at the bottom of this image, and the source extended beyond this edge. The ROIs used to calculate percentage background variability are seen in Figure 2. Table 2 lists the percentage background variability for uniform images of different acquisition durations and for the 12- and 24-slice images.

Counting-Rate Linearity

The recorded prompt-minus-random and random coincidence counts are plotted as a function of phantom activity concentration in Figure 3A. The dashed line through prompt-minus-random events is a linear fit to the low-concentration values; the line then extends to higher concentrations. The gray curve through the random events is a quadratic fit to all the measured random events data points. Random coincidence events were 0.62% and 7.3% of the total number of prompt events for 0.34 kBq/mL and 10 kBq/mL in the phantom, respectively. With no activity in the FOV (blank scan), the random events reported by the system were 0.74% of total prompts.

Edge Effects

A comparison of the true source position, as measured from the edge of the detector housing, with the image position taken from an in-plane image, showed that the accurate active imaging area of the PEM Flex Solo II begins at approximately 13 mm from the edge of the detector housing.

The COV and mean of image profiles parallel to and near the posterior edge of in-plane images are plotted as a function of distance from the edge of the detector housing in Figure 3B. The vertical gray line indicates where accurate positioning begins. The COV increases at the FOV edge as expected because of the limited coincidence sampling there.

RCs

Figure 4A shows 2 images, each with 4 of the spheres used in RC experiments. These images illustrate visualization of various sizes of spheres with 4× and 10× background activity concentration. These images were not used to calculate RCs; we measured RCs from images with spheres nearer the FOV center. Profiles through the 10× spheres and adjacent background are shown in Figure 4B. All 4 spheres are seen in the profile plot; however, the 4-mm spheres would likely not be distinguished from edge artifacts if they were closer to the edge.

Figure 5 shows the RC values plotted against sphere diameter. As expected, the measured RC values approach the true activity concentration ratio for larger sphere sizes. The RC values differed when the spheres were centered between the detectors versus being placed on 1 of the detectors; the on-detector relative RC_{max} (Eq. 1) appears to level out just above the true ratio value, whereas the FOV-centered RC_{max} curves level out below the true ratio value. The relative RC_{mean} (Eq. 2) and absolute RC_{max} (Eq. 3) followed similar trends.

NIH-PA Author Manuscript

NIH-PA Author Manuscript

NIH-PA Author Manuscript

Imaging of the 2-cm-diameter sphere at the 4 cardinal locations within the FOV (Fig. 1C) yielded the relative activity concentration values given in Table 3. As with the RC measurements, the measured activity concentration was found to be greater when the source was positioned on the detectors (positions ii and iv) than when centered between the detectors (i and iii). There is also a trend toward higher measured activity at the FOV edge relative to the center. The background activity was present for these experiments but did not figure into the calculation; the relative values reported here are from ROIs drawn entirely inside the sphere and normalized to their own respective (mean or maximum) highest value.

Clinical Examples

The patient images presented here represent anecdotal cases illustrating issues relevant to PEM imaging technology and technique.

Figure 6A shows the WB PET, PEM, MRI, and photograph of corresponding tissue of a patient with a known primary tumor in the right breast. The primary tumor was 2.6 cm with a maximum standardized uptake value of 5.4 g/mL on the WB PET image. The PEM lesion maximum to background was 12.6 on the MLO view, which was acquired 45 min after the WB image. PEM and MRI images showed a small second lesion (5 mm) with uptake significantly above background (PEM lesion maximum to background, 3.8); the second lesion was less evident on the WB PET image. Also visualized was an area of moderate ^{18}F-FDG uptake following ductal patterns, suggesting ductal carcinoma in situ (DCIS). These findings were supported by MRI and confirmed on pathologic examination.

Figures 6B-6C show 2 cases in which a lesion with high ^{18}F-FDG uptake was located in a posterior position. In 1 case (Fig. 6B), the lesion appeared on the edge of the craniocaudal view and approximately 1 cm from the edge of the MLO view, suggesting that MLO views can image more posterior tissue. In this case, the lesion is sufficiently large and sufficiently radioactive to be easily distinguished from the edge artifacts.

Figure 6C shows another posterior lesion, except in this patient the lesion was seen only on the MLO view and not on the craniocaudal view. Again, this lesion is sufficiently large and radioactive to be distinguished from edge artifacts. However, the accuracy of localizing this lesion in the mediolateral dimension suffers without visualization provided by the craniocaudal view.

DISCUSSION

No standards exist for testing dedicated breast PET or PEM systems. We selected performance parameters that could be measured with the standard clinical software on the PEM Flex Solo II and that were relevant to the breast imaging application. All analyses were performed on images reconstructed using the default MLEM method.

We measured 2.4 ± 0.3 mm FWHM spatial resolution for in-plane image slices, in agreement with the study by Luo et al. (15). We measured 8.0 ± 1.0 mm FWHM in the cross-plane images, a slightly greater FWHM than that found by Luo et al. (15) (7 mm FWHM). This is the primary advantage of the PEM Flex system; the improved spatial resolution allows visualization of finer details of tracer distribution than can be seen with WB scanners. The source used for these measurements was 1.0 mm in diameter. In this case, the source size and the image pixel size both affected the measured in-plane resolution. A reduced source size and image pixel size could result in a narrower in-plane point spread function. The fact that the measured performance can depend on the experimental methods illustrates the need for standards for characterizing dedicated PET systems. As has been done for clinical and preclinical PET

NIH-PA Author Manuscript

NIH-PA Author Manuscript

NIH-PA Author Manuscript

scanners, an appropriate NEMA testing standard should be developed for positron emission imaging systems that are dedicated to breast imaging.

Cross-plane images are not intended for viewing. At the Swedish Cancer Institute, 2 nearly orthogonal imaging views (craniocaudal and MLO) are acquired clinically to obtain high-resolution imaging in all 3 dimensions. Drawbacks to this protocol include an increased imaging time and breast compression in different directions for each of these views. As such, the 2 images are of a single object but distorted into 2 different shapes, making it challenging to correlate findings between the 2 PEM images and between mammographic, ultrasound, and MR images, each of which images the breast in its own distinct shape.

The percentage background variability was measured between approximately 5% and 7%, depending on acquisition time. Theoretically, the percentage background variability should decrease with increased acquisition duration because of the corresponding increase in counting statistics. Also, the percentage background variability is expected to be lower on the 12-slice images because of increased averaging. The expected trends were not observed on these images, indicating that the within-image variability predominates the counting statistics variance. The focal-plane tomography method of the PEM Flex is a likely contributor to the nonuniformity. The default image reconstruction does not include corrections for attenuated or scattered photons, which can also lead to nonuniformities in reconstructed images.

The coincidence counting rate increased linearly with activity concentration up to 2 kBq/mL in the phantom (Fig. 3A). This was measured using a 1.0-L phantom, approximately 800 mL of which was in the PEM Flex FOV. Breast sizes vary considerably. Eight hundred milliliters is representative of neither the largest nor the smallest breast but is within the typical volume of tissue seen in this application. Activity concentration expected in the breast ranges from approximately 3 to 5 kBq/mL. Again, there is a need to establish an appropriate counting-rate measurement metric for breast imaging PEM/PET systems that encompasses expected activity levels. The PEM Flex uses lutetium yttrium orthosilicate scintillation crystals that contain intrinsic radioactivity giving rise to additional prompt events detection. As such, counting-rate characterization of the PEM Flex must account for this activity, for example, as suggested in the study by Watson et al. (20).

Measured counting rates deviate from the ideal linear relationship with activity in all systems because of electronics counting-rate limitations. It is important to correct for the count losses to achieve quantitative accuracy. In limited-angle sampling systems such as the PEM Flex, there are other factors inhibiting the quantitative accuracy, making it difficult to discern the degree to which dead-time count losses affect quantification.

The COV in the PEM images increases at the edge of the FOV because of limited coincidence-count sampling at these positions (Fig. 3B). In WB PET, the effect of low sensitivity at the edge of the axial FOV is overcome by overlapping adjacent bed position acquisitions. This approach is not possible with a PEM system because the torso of the patient prevents positioning the detectors such that the posterior breast is in the center of the FOV. There is a trade-off between extending the PEM FOV and limiting image variance at the edge: using all image planes that the PEM detector can measure gives the maximum FOV but results in high variance at the FOV edge. This effect is seen as artifacts at the edges of the PEM Flex images (e.g., Figs. [2], 4A, and 6A–6C). However, as illustrated in Figures 6B–6C, maximizing the FOV can be important for patient imaging, despite the image artifacts at the edge. In the examples in Figures 6B–6C, the lesions were sufficiently large and had sufficient tracer uptake to be easily distinguished from the variance artifacts. Had these image slices been omitted for the sake of reducing overall image variance, then those lesions may not have been visualized. Maximizing the FOV is therefore important, with proper care at interpreting the edge of the

NIH-PA Author Manuscript

NIH-PA Author Manuscript

NIH-PA Author Manuscript

images. This is an area for further consideration concerning the design, evaluation, and implementation of dedicated breast PET and PEM systems.

Figure 4 suggests that to visualize lesions with uptake approximately 4 times the background tracer concentration, then the lesion must be approximately 5 mm or larger, and that a 4-mm sphere can be seen if its tracer concentration is approximately 10 times the background concentration. We note that these limits of visualization likely change at the extreme posterior edge of the PEM images; Figure 4B shows background noise near the FOV edge comparable to the 4-mm sphere with 10× background.

We performed a simple test of the shielding at the edge of the PEM Flex detectors to investigate random coincidence events from outside the FOV. The relative number of random coincidence events did not change appreciably when we placed additional shielding between the detector and the source outside the FOV. Contamination from outside-FOV activity is another effect that should be included in standardized testing of dedicated breast PET and PEM systems.

PEM hardware and data acquisition differ from conventional WB PET in several ways. Most obviously, PEM systems are much smaller. The development of testing standards for PEM systems requires the definition of test objects suitable in size for the detectors. With the definition of appropriate phantom sizes, the WB PET standards (19) encompass characterizations that should be included in tests of PEM scanners. In addition, the PEM detector arrangement, which is in contact with or very close to the breast, leads to considerable activity just outside the FOV (from the body) and prohibits placing posterior-breast and chest-wall tissue in the center of the PEM FOV. These unique features warrant additional PEM-specific standard tests that address performance with respect to these challenges. Variance at the edge of the FOV and random coincidence counts originating from outside of the FOV are 2 such parameters that should be characterized.

Our methods effectively demonstrated many of the imaging characteristics of the PEM Flex system. However, our methods were not optimized for standardized testing; for example, our spatial resolution calculation, and the use of intravenous bags for background activity are not recommended for general testing. We used acquisition and processing tools available on the PEM Flex clinical software in a clinical environment that is not equipped for detector experimentation. Certain metrics, such as absolute counting-rate sensitivities, require more access to raw data than is needed clinically. Typically, manufacturers provide specialized protocols for conducting standardized tests, but the tests must first be established.

Not all PEM systems will use the same detector geometry as the PEM Flex Solo II (7), but the distinctions from WB PET listed above apply generally, whether the PEM design uses the PEM Flex Solo II approach, a 4-detector approach, or a small-ring approach. Standardized breast PET/PEM tests should be general enough to accommodate alternative detector geometry. Table 4 lists a suggested guideline for establishing dedicated breast PET/PEM standardized testing.

The phantoms used for standardized PEM testing would be not only smaller than those used for WB PET systems but also structured differently to reflect the imaging tasks of PEM. Of less importance on a PEM system is an evaluation of activity recovery in low-density tissue (lung) or high-density tissue (bone), because these tissues likely are not viewed by PEM systems. High-counting-rate tasks are not currently part of breast imaging protocols, making the requirements for counting-rate linearity less stringent than in WB PET. Characterizing counting-rate performance of a PEM scanner is still important.

NIH-PA Author Manuscript

NIH-PA Author Manuscript

NIH-PA Author Manuscript

CONCLUSION

We performed several experiments to characterize a commercial PEM scanner, the PEM Flex Solo II from Naviscan PET Systems, Inc. The PEM Flex Solo II provides high-resolution dedicated breast images that show greater tracer uptake detail than can be seen with standard WB PET scanner protocols. The high resolution allows visualization of approximately 4-mm-diameter objects if they have 10× background activity concentration and approximately 6- to 7-mm objects if the activity is 4 times the background. The PEM scanner is well suited to identifying multifocal and multicentric disease, which is an important consideration for treatment planning. DCIS uptake is also frequently seen with this resolution. PEM Flex image quantification was variable within the FOV (Table 3), making quantitation measurements challenging from a reproducibility standpoint. Adding attenuation and scatter correction should improve quantification, yet fundamental limitations will persist because of the limited-angle sampling.

As interest in dedicated breast PET increases, and more systems are developed and placed in clinics, a standard method for comparing and characterizing systems must be developed. As was done for small-animal PET scanners, a modified form of the WB PET testing standard should be developed that takes into account the size and configuration of dedicated breast scanners and includes tests specifically relevant to breast imaging, such as edge detection and random coincidences from outside the FOV.

Acknowledgments

We thank Chris Matthews of Naviscan for useful discussions and Jennifer Coburn, Joiem Kawas, and Kris Kohn of the Swedish Cancer Institute for their assistance with experiments. We also thank Bruce Porter, Swedish First Hill Diagnostic Imaging, Seattle, WA, for the MRI figure. This work is supported by NIH grant R01-CA74135.

REFERENCES

1. Tabar L, Vitak B, Chen H-H, et al. Beyond randomized controlled trials: organized mammographic screening substantially reduces breast carcinoma mortality. Cancer 2001;91:1724–1731. [PubMed: 11335897]
2. Wahl RL, Cody RL, Hutchins GD, Mudgett EE. Primary and metastatic breast carcinoma: initial clinical evaluation with PET with the radiolabeled glucose analogue 2-[F-18]-fluoro-2-deoxy-d-glucose. Radiology 1991;179:765–770. [PubMed: 2027989]
3. Avril N, Rose CA, Shelling M, et al. Breast imaging with positron emission tomography and fluorine-18 fluorodeoxyglucose: use and limitations. J Clin Oncol 2000;18:3495–3502. [PubMed: 11032590]
4. Eubank WB, Mankoff DA. Current and future uses of positron emission tomography in breast cancer imaging. Semin Nucl Med 2004;34:224–240. [PubMed: 15202103]
5. Thompson CJ, Murthy K, Weinberg IN, Mako F. Feasibility of positron emission mammography. Med Phys 1994;21:529–538. [PubMed: 8058019]
6. Wang G-C, Huber JS, Moses WW, et al. Characterization of the LBNL PEM camera. IEEE Trans Nucl Sci 2006;53:1129–1135.
7. Raylman RR, Majewski S, Smith M, et al. The positron emission mammography/tomography breast imaging and biopsy system (PEM/PET): design, construction and phantom-based measurements. Phys Med Biol 2008;53:637–653. [PubMed: 18199907]
8. Abreu MC, Aguiar JD, Almeida FG, et al. Design and evaluation of the Clear-PEM scanner for positron emission mammography. IEEE Trans Nucl Sci 2006;53:71–77.
9. Murthy K, Aznar M, Thompson CJ, et al. Results of preliminary clinical trials of the positron emission mammography system PEM-I: a dedicated breast imaging system producing glucose metabolic images using FDG. J Nucl Med 2000;41:1851–1858. [PubMed: 11079494]
10. Levine EA, Freimanis RI, Perrier ND, et al. Positron emission mammography: initial clinical results. Ann Surg Oncol 2003;10:86–91. [PubMed: 12513966]

NIH-PA Author Manuscript

NIH-PA Author Manuscript

NIH-PA Author Manuscript

11. Rosen EL, Turkington TG, Soo MS, et al. Detection of primary breast carcinoma with dedicated, large-field-of-view FDG PET mammography device: initial experience. Radiology 2005;234:527–534. [PubMed: 15671006]
12. Tafra L, Cheng Z, Uddo J, et al. Pilot clinical trial of ^{18}F-fluorodeoxyglucose positron-emission mammography in the surgical management of breast cancer. Am J Surg 2005;190:628–632. [PubMed: 16164937]
13. Berg WA, Weinberg IN, Narayanan D, et al. High-resolution fluorodeoxyglucose positron emission tomography with compression ("positron emission mammography") is highly accurate in depicting primary breast cancer. Breast J 2006;12:309–323. [PubMed: 16848840]
14. Quon A, Gambhir SS. FDG-PET and beyond: molecular breast cancer imaging. J Clin Oncol 2005;23:1664–1673. [PubMed: 15755974]
15. Luo W, Anashkin E, Matthews CG. First test results of a commercially available clinical PET scanner using the NEMA NU 4-2008 small animal PET standards. IEEE Nucl Sci Symp Conf Rec 2008:4718–4723.
16. Dobbins JT, Godfrey DJ. Digital x-ray tomosynthesis: current state of the art and clinical potential. Phys Med Biol 2003;48:R65–R106. [PubMed: 14579853]
17. Huang S-C. Anatomy of SUV. Nucl Med Biol 2000;27:643–646. [PubMed: 11091106]
18. Rosset A, Spadola L, Ratib O. OsiriX: an open-source software for navigating in multidimensional DICOM images. J Digit Imaging 2004;17:205–216. [PubMed: 15534753]
19. National Electrical Manufacturers Association. Performance Measurements of Positron Emission Tomographs. National Electrical Manufacturers Association; Rosslyn, VA: 2001. NEMA standards publication NU 2-2001
20. Watson CC, Casey ME, Eriksson L, et al. NEMA NU 2 performance tests for scanners with intrinsic radioactivity. J Nucl Med 2004;45:822–826. [PubMed: 15136632]

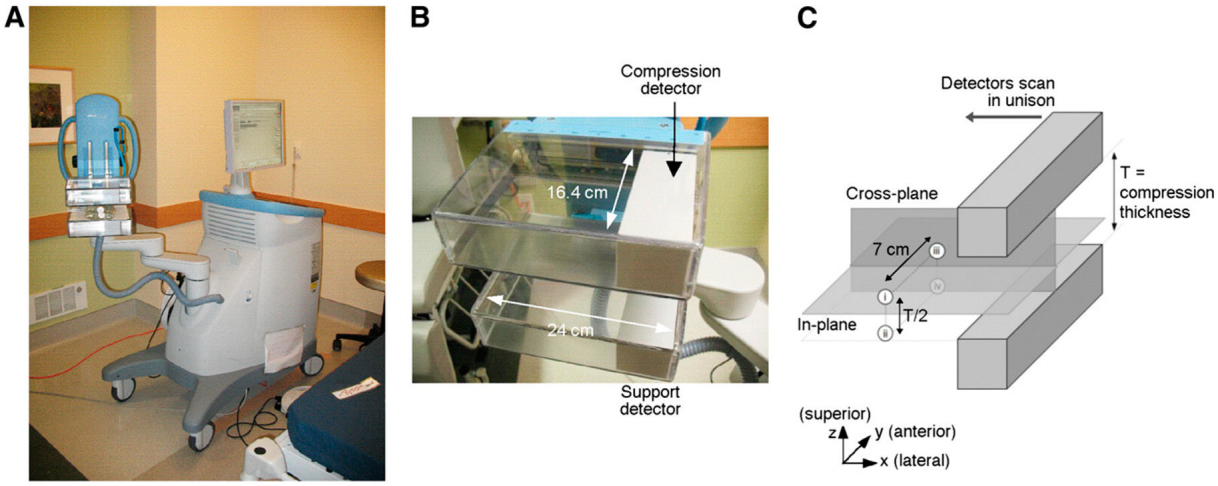

FIGURE 1.
(A) PEM Flex Solo II system. (B) Close-up of detectors. (C) Illustration of in-planes and cross-planes. Four cardinal positions (i, ii, iii, and iv) within PEM Flex FOV used to investigate quantification consistency.

NIH-PA Author Manuscript
NIH-PA Author Manuscript
NIH-PA Author Manuscript

NIH-PA Author Manuscript

NIH-PA Author Manuscript

NIH-PA Author Manuscript

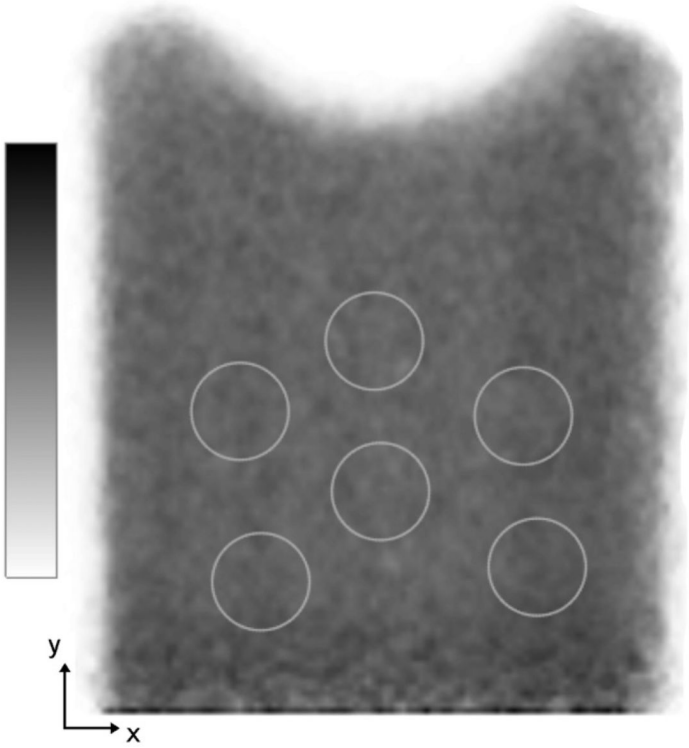

FIGURE 2.
Uniform source image showing ROIs used to calculate percentage background variability. Source extends beyond detector at bottom of this figure.

NIH-PA Author Manuscript

NIH-PA Author Manuscript

NIH-PA Author Manuscript

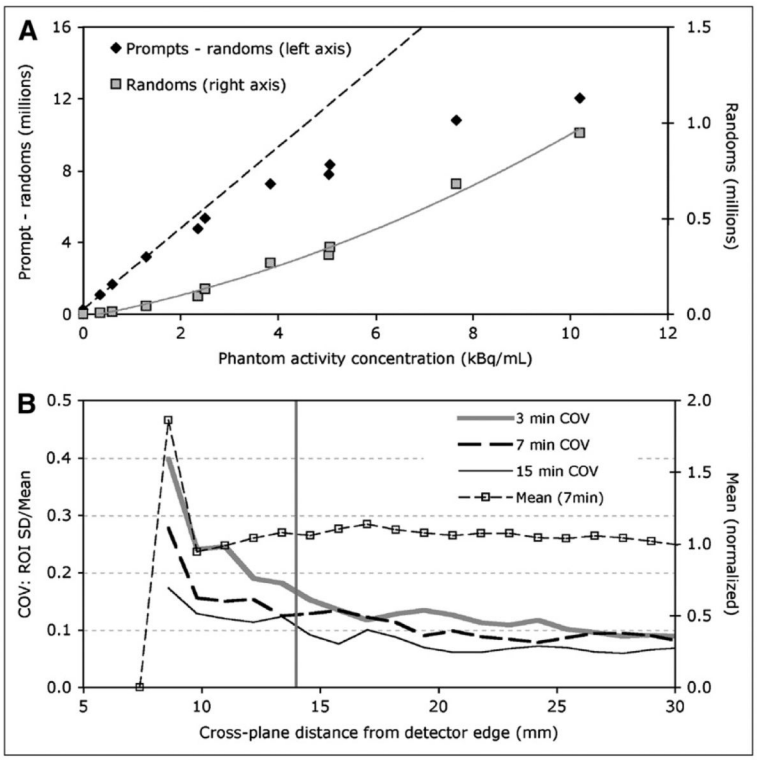

FIGURE 3.

(A) Prompt-minus-random and random coincidence events. (B) From 1-dimensional profiles described in text, COV from 3-, 7-, and 15-min acquisitions and mean from 7-min acquisition. Vertical gray line indicates beginning of accurate positioning linearity.

NIH-PA Author Manuscript

NIH-PA Author Manuscript

NIH-PA Author Manuscript

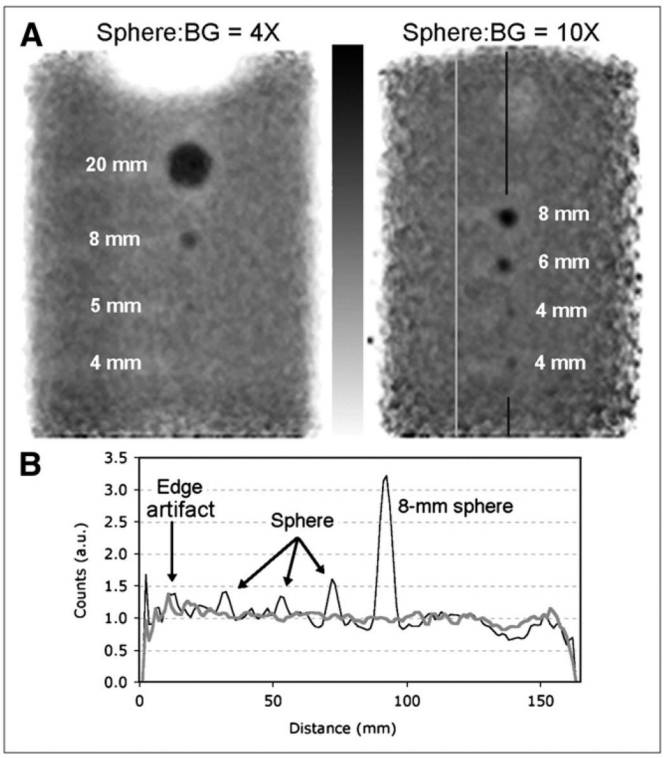

FIGURE 4.

(A) Sphere sources in background. Sphere-to-background activity concentration ratio and sphere diameters are indicated. Vertical lines on right-hand image show location of profiles in B. (B) Profile through 10× spheres (black curve) and profile through adjacent background (gray curve).

NIH-PA Author Manuscript
NIH-PA Author Manuscript
NIH-PA Author Manuscript

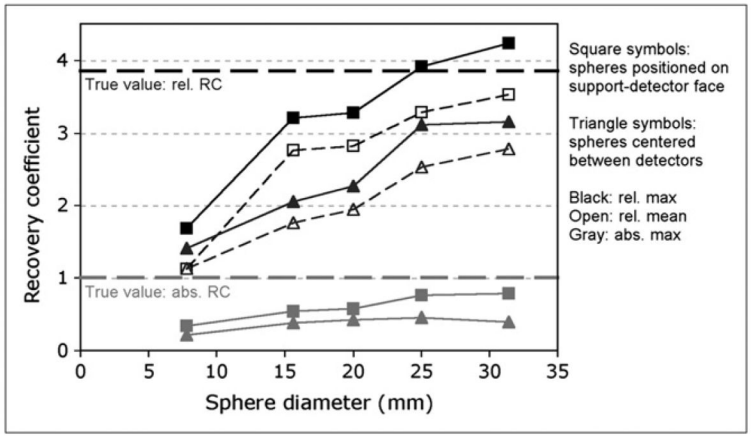

FIGURE 5.

Relative RCs (Eqs. 1 and 2) are shown in black. Absolute RCs (Eq. 3) are in gray. True activities: 16–22 kBq/mL in spheres and 4.3–5.9 kBq/mL in background.

NIH-PA Author Manuscript
NIH-PA Author Manuscript
NIH-PA Author Manuscript

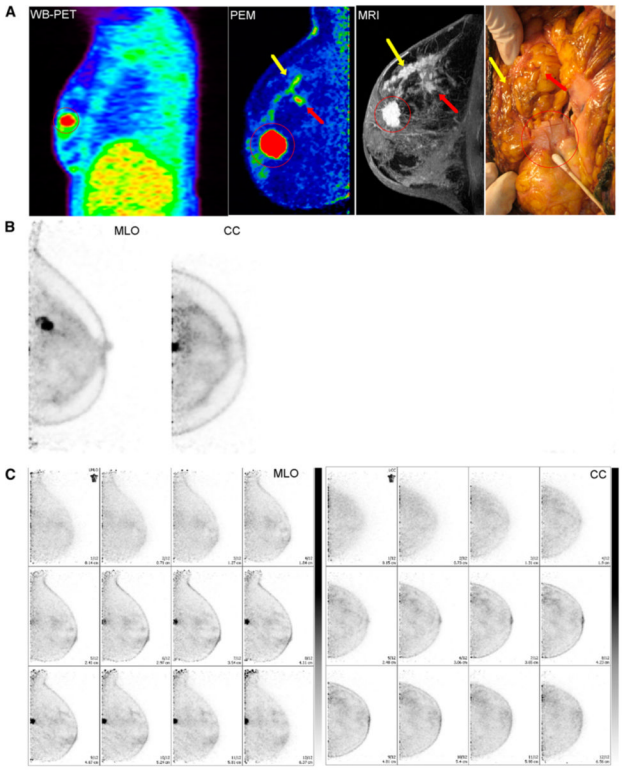

FIGURE 6.

(A) Case 1: WB PET identifies index lesion (red circle). PEM and MRI (gadolinium-enhanced, T1 fat-saturated) show secondary lesion (red arrow) and DCIS (yellow arrow). Pathology-confirmed PEM/MRI findings (photo is of gross breast anatomy corresponding to imaging tomographic sections). (B) Case 2: posterior lesion is seen on MLO and craniocaudal views and is clearly distinguished from edge-variance artifacts. (C) Case 3: posterior lesion seen on MLO but not on craniocaudal view. Case 2 and 3 show MLO view imaging farther posterior than CC view.

NIH-PA Author Manuscript

NIH-PA Author Manuscript

NIH-PA Author Manuscript

TABLE 1

Spatial Resolution

Compression thickness (cm)	Spatial resolution FWHM (mm)	
	In-plane*	Cross-plane
3	2.58 ± 0.28	8.50 ± 0.32
6	2.45 ± 0.32	7.34 ± 0.64
9	2.39 ± 0.29	9.23 ± 0.65

*In-plane resolution is isotropic.

NIH-PA Author Manuscript

NIH-PA Author Manuscript

NIH-PA Author Manuscript

TABLE 2

Percentage Background Variability

	% Background variability	
Acquisition duration (min)	**24-slice**	**12-slice**
1	5.1	4.6
3	5.6	5.5
7	7.0	6.8
15	6.0	6.2

NIH-PA Author Manuscript

NIH-PA Author Manuscript

NIH-PA Author Manuscript

TABLE 3

PEM Standardized Uptake Value Consistency

Position*	Mean†	Maximum†
i	74	68
ii	100	100
iii	65	60
iv	89	79

*Positions are shown in Figure 1C.

†Mean and maximum normalized to respective highest values.

NIH-PA Author Manuscript

NIH-PA Author Manuscript

NIH-PA Author Manuscript

TABLE 4

Proposed Metrics for Standardized Dedicated Breast PET/PEM Evaluation

Guideline	Task
Initial task	Define phantoms appropriate for PEM-size scanner
Tests common to WB PET scanners	Spatial resolution
	Sensitivity (counting rate per activity)
	RC vs. object size
	Percentage background variability
	Counting rate limitations, and count-loss corrections
Additional PEM-specific tests	Quantification consistency within the FOV
	Random coincidences from outside FOV
	Variance at the edge of the FOV
	Image position-to-physical space calibration accuracy for biopsy guidance